References

[1] Rogers, T. G. and Lee, E. H., "The Cylinder Problem in Viscoelastic Stress Analysis," *Quarterly of Applied Mathematics*, Vol. 22, 1964, p. 117.

[2] Huang, N. C., Lee, E. H., and Rogers, T. G., "On the Influence of Viscoelastic Compressibility in Stress Analysis," *Proceedings of the 4th International Congress on Rheology*, Vol. 2, 1965, p. 213.

[3] Ting, T. C. T., "Remarks on Linear Viscoelastic Stress Analysis in Cylinder Problems," *Proceedings of the 9th Midwestern Mechanics Conference*, 1965, p. 263.

[4] Volterra, V., *Theory of Functionals*, Dover, New York, 1959.

[5] Shinozuka, M., "Stresses in a Linear Incompressible Viscoelastic Cylinder with Moving Inner Boundary," *Journal of Applied Mechanics*, Vol. 30, 1963, p. 335.

[6] Lee, E. H. and Rogers, T. G., "Solution of Viscoelastic Stress Analysis Problems Using Measured Creep or Relaxation Functions," *Journal of Applied Mechanics*, Vol. 30, 1963, p. 127.

[7] Williams, M. L., "Structural Analysis of Viscoelastic Materials," *AIAA Journal*, Vol. 2, No. 5, May 1964, pp. 785–808.

JANUARY 1970 AIAA JOURNAL VOL. 8, NO. 1

Buckling of Elliptic Cylinders under Normal Pressure

JOHN C. YAO* AND WILLIAM C. JENKINS†
McDonnell-Douglas Astronautics Company—Western Division, Santa Monica, Calif.

An analytical and experimental investigation was conducted to determine the buckling behavior of elliptic cylinders under normal pressure. Tests were performed on a total of 80 models made of polyvinyl-chloride sheet. The models were simply supported and the buckling mode was found as an oval dimple which appears around the surface with the least curvature. Theoretical buckling pressure was also obtained by using Goldenveizer's linear, thin-shell theory in conjunction with Galerkin's method for solution. The test data and theory agree fairly well, provided that the shell is not too short or too thick. For design purposes, curves are provided in nondimensional form to show the interaction of the physical quantities of the cylinders and the buckling pressures obtained by theory as well as by experiment.

Nomenclature

a	=	semimajor axis of ellipse
b	=	semiminor axis of ellipse
d	=	half of periphery of ellipse
dA	=	surface element
E	=	Young's modulus
l	=	length
M_x	=	moment at ends due to buckling displacements
n	=	circumferential wave number
p	=	normal pressure
R	=	radius of curvature of ellipse
r	=	a^2/b (radius of curvature of ellipse at its minor axis)
s	=	β/l
t	=	thickness
T_x'	=	axial membrane force at the ends due to buckling displacements
$T_x, T_x,$ $T_{x\alpha}, T_{sx}$	=	prebuckling membrane forces (Fig. 2)
u	=	u'/t
v	=	v'/t
w	=	w'/t
u', v', w'	=	buckling displacements along α, β, and z, directions: w' is positive if inward
x	=	α/l
α, β, z	=	curvilinear coordinate system (Fig. 1)
λ	=	$(1 - \nu^2)(l/t)(p/E)$(buckling parameter)
ν	=	Poisson's ratio
ϕ	=	angle between normal and semiminor axis (Fig. 3)

Introduction

THE strongest and yet the lightest shell structure for bearing normal external pressure is undoubtedly a sphere; however, the requirement for a structure to perform functions other than carrying pressure often forces us to consider other shell configurations. The cylindrical shell of elliptic cross section is one such configuration.

The present paper is concerned with the buckling of elliptical cylinders with simply supported ends. This problem has been considered before by B. I. Slepov.[1] However, it appeared necessary to reopen the investigation for the following reasons: 1) Slepov expressed the buckling mode as a Fourier series but used only one term in the analysis, which is too crude an approximation for good accuracy. 2) Slepov's theoretical analysis was supported by only two test points, which is insufficient to confirm the theory or establish any trend. 3) no design criterion incorporating the deviation between theoretical and test results has yet been established.

In this investigation, a total of 80 models made of polyvinyl-chloride (PVC) sheet were buckled in a test program carried out by the second author. The analytical work was performed by the first author, who used Goldenveizer's thin-shell theory[2] and Galerkin's method for solution. The buckling prediction made from this investigation is presented in graphical form with a wide range of geometric and material parameters.

Theory

We chose the coordinate system α and β along the lines of curvature on the middle surface of the shell and z the normal to the middle surface as shown in Fig. 1. Let t and l be the wall thickness and length of the shell, respectively, and let u', v', and w' be the buckling displacements of a point on the middle surface along the α, β, and z directions, respectively, with w' considered as positive if inward. Accordingly, we adopted the following nondimensional quantities in the sequel:

$$x = \alpha/l, \quad s = \beta/l, \quad u = u'/t$$
$$v = v'/t, \quad w = w'/t \tag{1}$$

Received February 18, 1969; revision received July 9, 1969.

* Principal Scientist, Advance Structures and Mechanical Department; now at Douglas Aircraft Company, Long Beach, Calif.

† Supervisor, Advance Structures and Mechanical Department.

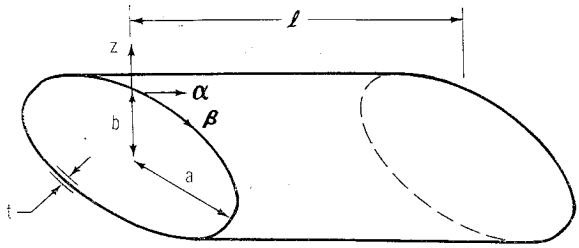

Fig. 1 Elliptic cylinder.

According to Goldenveizer,[2] the three equations of equilibrium for an elliptic cylinder under normal pressure at the onset of buckling may be expressed in the form‡

$$\frac{\partial^2 u}{\partial x^2} + \frac{1-\nu}{2}\frac{\partial^2 u}{\partial s^2} + \frac{1+\nu}{2}\frac{\partial^2 v}{\partial x \partial s} - \nu\frac{l}{R}\frac{\partial w}{\partial x} = 0 \quad (2)$$

$$\frac{1+\nu}{2}\frac{\partial^2 u}{\partial x \partial \beta} + \frac{\partial^2 v}{\partial s^2} + \frac{1-\nu}{2}\frac{\partial^2 v}{\partial x^2} - \frac{\partial}{\partial s}\left(\frac{l}{R}w\right) + \frac{1}{12}\frac{l}{R}\left(\frac{t}{l}\right)^2\frac{\partial}{\partial s}\left(\frac{\partial^2 w}{\partial x^2} + \frac{\partial^2 w}{\partial s^2}\right) = 0 \quad (3)$$

$$\left(\frac{l}{R}\right)\left(\nu\frac{\partial u}{\partial x} + \frac{\partial v}{\partial s} - \frac{l}{R}w\right) + \frac{1}{12}\left(\frac{t}{l}\right)^2 \times \left\{\frac{1-\nu}{2}\frac{\partial}{\partial s}\left(\frac{l}{R}\frac{\partial}{\partial x}\right)\left(\frac{\partial u}{\partial s} - \frac{\partial v}{\partial x}\right) - \left(\frac{\partial^2}{\partial x^2} + \frac{\partial^2}{\partial s^2}\right) \times \frac{\partial}{\partial s}\left(\frac{l}{R}v\right) - \left(\frac{\partial^2}{\partial x^2} + \frac{\partial^2}{\partial y^2}\right)^2 w\right\} + (1-\nu^2)\left(\frac{l}{t}\right)^2\frac{Z}{E} = 0 \quad (4)$$

where R is the radius of curvature, ν and E are Poisson's ratio and Young's modulus, respectively, and§

$$Z = \frac{t}{l^2}\left\{\frac{\partial}{\partial x}\left(T_x\frac{\partial w}{\partial x}\right) + \frac{\partial}{\partial s}\left[T_s\left(\frac{\partial w}{\partial s} + \frac{l}{R}v\right)\right] + \frac{\partial}{\partial x}\left[T_{xs}\left(\frac{\partial w}{\partial s} + \frac{l}{R}v\right)\right] - \frac{\partial}{\partial s}\left(T_{sx}\frac{\partial w}{\partial x}\right) + \frac{1}{2}T_{sx}\left(\frac{l}{R}\right)\left(\frac{\partial u}{\partial s} - \frac{\partial v}{\partial x}\right)\right\} \quad (5)$$

In Eq. (5), T_x, T_s, T_{xs}, and T_{sx} are prebuckling membrane forces as illustrated in Fig. 2.

The prebuckling membrane forces appearing in Eq. (5) are now obtained by membrane theory.[4] Assuming that the boundary conditions for a cylindrical shell of elliptic cross section are given by

$$T_x = 0, \quad v = 0 \quad (6)$$

its prebuckling membrane forces due to external normal pressure p are found as

$$T_x = -plx[(x-1)/2](d^2/ds^2)(R/l)$$
$$T_s = -pl(R/l) \quad (7)$$
$$S_{xs} = -S_{sx} = -pl(\tfrac{1}{2} - x)(d/ds)(R/l)$$

For the sake of completeness and for the purpose of later computation, it is appropriate to record some of the properties of an ellipse before we proceed to discuss the solution to this problem. We write the radius of curvature R and the nondimensional arc-length s as follows:

$$R/l = (b^2/al)[1/(1 - \epsilon^2\cos^2\phi)^{3/2}]$$
$$\epsilon^2 = 1 - \left(\frac{b}{a}\right)^2, \quad s = \int_0^\phi \left(\frac{R}{l}\right)d\phi \quad (8)$$

‡ Terms containing $(t/R)^2 \ll 1$ are omitted from this paper.

§ See expression for rotation components on p. 53, Ref. 2.

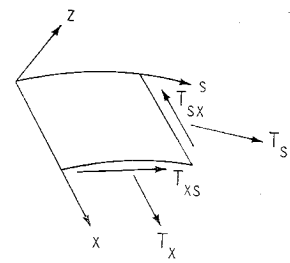

Fig. 2 Prebuckling membrane forces.

where a and b are the semimajor and minor axes of the ellipse and ϕ is the angle between a normal to the ellipse and the semiminor axis as shown by Fig. 3.

From the test results (Fig. 4), it was found that the buckling pattern is a single oval-shape dimple situated near the semiminor axis. Along the axial direction, it assumes the shape of a half sine wave. For this reason, we let the buckling deformation take the following form¶:

$$u = \cos x\pi \sum_n A_n \cos n\left(\frac{s}{d}\right)\pi$$
$$v = \sin x\pi \sum_n B_n \sin n\left(\frac{s}{d}\right)\pi \quad (n = 2,3,4,\ldots) \quad (9)$$
$$w = \sin x\pi \sum_n C_n \cos n\left(\frac{s}{d}\right)\pi$$

where $2d$ is the periphery of the ellipse.

To study the permissible boundary conditions implied by Eq. (9), we need to know the bending moment M_x in the x-z plane and the membrane force T'_x due to buckling displacements.

From Hooke's law and the strain-displacement relationship (see Ref. 2, pp. 52–54 and 96), it is found that the moment M_x is given by

$$M_x = \frac{-Et^4}{12(1-\nu^2)l^2}\left[\frac{\partial^2 w}{\partial x^2} + \nu\frac{\partial^2 w}{\partial s^2} + \nu\frac{\partial}{\partial s}\left(\frac{l}{R}v\right)\right] \quad (10)$$

while the membrane force T'_x is given by

$$T'_x = \frac{Et^2}{(1-\nu^2)l}\left[\frac{\partial u}{\partial x} + \nu\left(\frac{\partial v}{\partial s} - \frac{l}{R}w\right)\right] \quad (11)$$

By combining Eqs. (9–11), it is found that at $x = 0, 1$ the permissible boundary conditions are

$$M_x = T'_x = v = w = 0 \quad (12)$$

The equilibrium conditions are therefore to be satisfied by Eq. (9) with as many terms as necessary for accuracy according to the method of Galerkin,[3] hence, we require

$$\iint_A \text{Eq. (2)}\cdot\delta A_n \cos x\pi \cos n\frac{s}{d}\pi dA = 0$$
$$\iint_A \text{Eq. (3)}\cdot\delta B_n \sin x\pi \sin n\frac{s}{d}\pi dA = 0 \quad (13)$$
$$\iint_A \text{Eq. (4)}\cdot\delta C_n \sin x\pi \cos n\frac{s}{d}\pi dA = 0$$
$$(n = 2,3,4,\ldots)$$

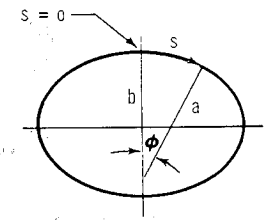

Fig. 3 Ellipse.

¶ Buckling modes of the form $w = \sin x\pi \sin n(s/d)\pi$ were also tried without yielding any new information.

The integration is carried out over the entire middle surface of the shell, but, since all the integrands are symmetric functions about the minor axis, the work of integration around the circumference can be reduced by half. After some algebraic work, we arrive at the following coupled simultaneous equations with A_n, B_n, and C_n as unknowns:

$$\frac{d}{4}\left[\pi^2+\frac{1-\nu}{2}\left(\frac{m\pi}{d}\right)^2\right]A_m-\frac{1+\nu}{8}m\pi^2B_m+\sum_n\frac{\nu}{2}\pi\int_0^\pi C_n\cos n\frac{s}{d}\pi\cos m\frac{s}{d}\pi d\phi=0 \qquad (m=2,3,4,\ldots) \quad (14)$$

$$\frac{1+\nu}{8}m\pi^2A_m-\frac{d}{4}\pi^2\left[\left(\frac{m}{d}\right)^2+\frac{1-\nu}{2}\right]B_m+\sum_n\int_0^\pi\frac{1}{2}C_n\left(n\frac{\pi}{d}\right)\left\{1+\frac{1}{12}\left(\frac{t}{l}\right)^2\left[\pi^2+\left(\frac{n\pi}{d}\right)^2\right]\right\}\times$$
$$\sin n\frac{s}{d}\pi\sin m\frac{s}{d}\pi d\phi-\sum_n\int_0^\pi\frac{1}{2}C_n\frac{\partial}{\partial s}\left(\frac{l}{R}\right)\cos n\frac{s}{d}\pi\sin m\frac{s}{d}\pi\left(\frac{R}{l}\right)d\phi=0 \qquad (m=2,3,4,\ldots) \quad (15)$$

$$\sum_n\frac{\pi}{2}\int_0^\pi A_n\left\{\left[\frac{1-\nu}{24}\left(\frac{t}{l}\right)^2\left(n\frac{\pi}{s}\right)^2-\nu\right]\cos n\frac{s}{d}\pi+\frac{1-\nu}{24}\left(\frac{t}{l}\right)^2\left(n\frac{\pi}{d}\right)\frac{\partial}{\partial s}\left(\frac{l}{R}\right)\sin n\frac{s}{d}\pi\right\}\cos m\frac{s}{d}\pi d\phi+$$
$$\sum_n\int_0^\pi B_n\left\{\frac{1}{2}\left(n\frac{\pi}{d}\right)+\frac{1}{24}\left(\frac{t}{l}\right)^2\left[\frac{3-\nu}{2}\pi^2\left(n\frac{\pi}{d}\right)+\left(n\frac{\pi}{d}\right)^3-3\left(\frac{R}{l}\right)\left(n\frac{\pi}{d}\right)\frac{\partial^2}{\partial s^2}\left(\frac{l}{R}\right)\right]\right\}\times$$
$$\cos n\frac{s}{d}\pi\cos m\frac{s}{d}\pi d\phi+\sum_n\int_0^\pi B_n\frac{1}{24}\left(\frac{t}{l}\right)^2\left[\frac{3-\nu}{2}\pi^2\frac{\partial}{\partial s}\left(\frac{l}{R}\right)-\frac{\partial^3}{\partial s^3}\left(\frac{l}{R}\right)+3\frac{\partial}{\partial s}\left(\frac{l}{R}\right)\left(n\frac{\pi}{d}\right)^2\right]\times$$
$$\sin n\frac{s}{d}\pi\cos m\frac{s}{d}\pi\cdot\left(\frac{R}{l}\right)d\phi-\frac{d}{48}\left(\frac{t}{l}\right)^2\left(\pi^2+m^2\frac{\pi^2}{d^2}\right)^2C_m-\sum_n\frac{1}{2}\int_0^\pi C_n\left(\frac{l}{R}\right)\cos n\frac{s}{d}\pi\cos m\frac{s}{d}\pi d\phi-$$
$$\lambda\sum_n\int_0^\pi C_n\left\{\left(\frac{1}{8}+\frac{\pi^2}{6}\right)\left(\frac{R}{l}\right)\frac{\partial^2}{\partial s^2}\left(\frac{R}{l}\right)-\frac{1}{2}\left(\frac{R}{l}\right)^2\left(n\frac{\pi}{d}\right)^2\right\}\cos n\frac{s}{d}\pi\cos m\frac{s}{d}\pi d\phi+\lambda\sum_n\int_0^\pi C_n\frac{1}{2}\left(\frac{R}{l}\right)\times$$
$$\left(n\frac{\pi}{d}\right)\frac{\partial}{\partial s}\left(\frac{R}{l}\right)\sin n\frac{s\pi}{d}\cos m\frac{s}{d}\pi d\phi-\frac{1}{4}\lambda m\pi B_m-\lambda\sum_n\int_0^\pi\frac{1}{8}\left[A_n\left(\frac{n}{d}\right)-B_n\right]\frac{\partial}{\partial s}\left(\frac{R}{l}\right)\times$$
$$\sin n\frac{s}{d}\pi\cos m\frac{s}{d}\pi d\phi=0 \qquad (m=2,3,4,\ldots) \quad (16)$$

where λ is the nondimensionalized eigenvalue containing the buckling pressure p, i.e.,

$$\lambda=(1-\nu^2)(l/t)(p/E) \qquad (17)$$

The integrations shown in Eqs. (14–16) are carried out numerically by Simpson's rule. The lowest buckling pressure p or the lowest eigenvalue λ is found from the determinant of the coefficients A_m, B_m, and C_m from this system of simultaneous equations. Enough terms (i.e., sufficient numbers of n) are used in Eq. (9) to include all the dominant eigenvectors in the calculation. We shall postpone the presentation of the numerical results thus found and discuss the experimental work.

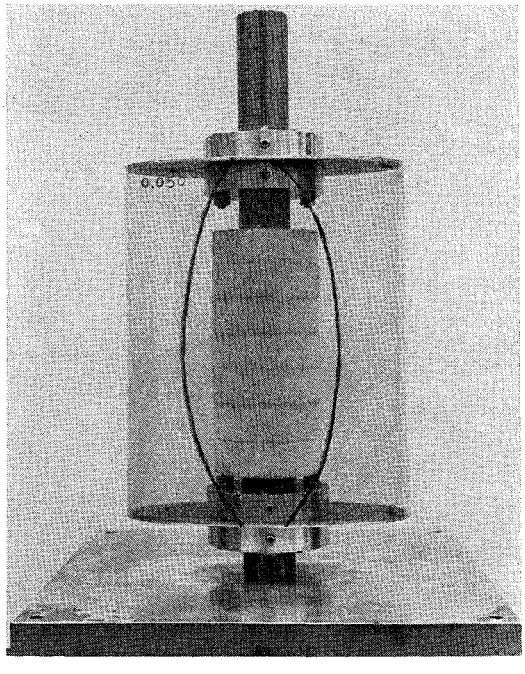

Fig. 4 A buckled elliptic cylinder.

Experiments

The models used in this experimental investigation were made from a rigid-vinyl PVC manufactured by the Union Carbide Company under the trademark "Bakelite." The material was purchased in sheet form.

The modulus of elasticity and Poisson's ratio were determined from tensile specimens. The tensile tests indicate the material to be nearly isotropic with the modulus of elasticity slightly affected by the thickness of the sheet. The material demonstrated little time dependence provided the strain rate was less than 0.02 in./in./min. The pertinent material properties are listed in Table 1.

The models were formed by molding PVC sheet over plaster mandrels which were shaped after a half-elliptic cylinder. The half-elliptic cylinders were formed by placing a sheet of PVC on the mandrel at room temperature, then raising the temperature to 200°F. At this temperature, the PVC sheet softened and draped itself over the mandrel. A thin sheet of silicone rubber which was weighted along two sides was then placed over the PVC sheet to insure that it was in intimate contact with the mandrel. The temperature was lowered slowly to room temperature and the formed PVC sheet could be removed from the mandrel.

Table 1 Material properties of PVC sheet

Heat distortion temperature, °F	160
Coefficient of thermal expansion, in./in./°F	0.0003
Tensile strength, lb/in.^{2}	8,000
Elongation at fracture, %	30
Poisson's ratio	0.37
Modulus of elasticity, lb/in.^{2}	470,000

Table 2 Theoretical and test data for elliptic cylinder under normal pressure[a]

t, in.	l, in.	r/t	r/l	$(1-\nu^2)(l/t)\times(p/E)\times 10^4$ Test	Theory	Test/Theory
0.018	2	444	4.00	1.03		
	4		2.00	1.16		
	6		1.33	1.24		
	8		1.00	1.34		
	10		0.80	1.24		
0.019	2	421	4.00	1.20	1.38	0.87
	4		2.00	1.25	1.28	0.98
	6		1.33	1.39	1.26	1.10
	8		1.00	1.46	1.28	1.14
	10		0.80	1.36	1.29	1.05
0.028	2	286	4.00	2.24		
	4		2.00	2.12		
	6		1.33	2.52		
	8		1.00	2.40		
	10		0.80	2.17		
0.029	2	276	4.00	2.36	2.82	0.84
	4		2.00	2.24	2.54	0.88
	6		1.33	2.51	2.51	1.00
	8		1.00	2.70	2.53	1.07
	10		0.80	2.60	2.47	1.05
0.049	2	163	4.00	...		
	4		2.00	4.07		
	6		1.33	4.50		
	8		1.00	4.20		
	10		0.80	4.11		
0.051	2	157	4.00	...	7.29	...
	4		2.00	4.53	6.23	0.73
	6		1.33	4.80	6.09	0.79
	8		1.00	4.44	5.86	0.76
	10		0.80	4.13	5.88	0.70
0.090	2	89	4.00	...		
	4		2.00	...		
	6		1.33	9.28		
	8		1.00	9.18		
	10		0.80	8.92		
0.091	2	88	4.00	...	20.40	...
	4		2.00	...	16.20	...
	6		1.33	9.39	15.10	0.62
	8		1.00	9.42	15.20	0.62
	10		0.80	8.97	16.60	0.54

[a] $a/b = 2.0$, $a = 4.000$ in., $b = 2.000$ in.

Table 3 Theoretical and test data for elliptic cylinder under normal pressure[a]

t, in.	l, in.	r/t	r/l	$(1-\nu^2)(l/t)\times(p/E)\times 10^4$ Test	Theory	Test/Theory
0.018	2	444	4.00	1.13		
	4		2.00	1.17		
	6		1.33	1.29		
	8		1.00	1.33		
	10		0.80	1.32		
0.019	2	421	4.00	1.16	1.32	0.88
	4		2.00	1.17	1.22	0.96
	6		1.33	1.23	1.20	1.03
	8		1.00	1.29	1.20	1.08
	10		0.80	1.28	1.21	1.06
0.029	2	276	4.00	2.05		
	4		2.00	2.15		
	6		1.33	2.31		
	8		1.00	2.55		
	10		0.80	2.53		
0.029	2	276	4.00	2.05	2.72	0.75
	4		2.00	2.19	2.41	0.91
	6		1.33	2.31	2.36	0.98
	8		1.00	2.50	2.36	1.06
	10		0.80	2.53	2.35	1.08
0.047	2	170	4.00	...		
	4		2.00	4.44		
	6		1.33	4.63		
	8		1.00	4.80		
	10		0.80	4.77		
0.049	2	163	4.00	...	7.08	0.75
	4		2.00	4.74	5.94	0.91
	6		1.33	5.10	5.72	0.98
	8		1.00	5.29	5.67	1.06
	10		0.80	5.42	5.69	1.08
0.088	2	91	4.00	...		
	4		2.00	...		
	6		1.33	11.04		
	8		1.00	11.60		
	10		0.80	11.20		
0.090	2	89	4.00	...	20.30	...
	4		2.00	...	15.60	...
	6		1.33	11.83	14.70	0.80
	8		1.00	12.31	14.50	0.85
	10		0.80	11.83	14.30	0.83

[a] $a/b = 1.5$, $a = 5.333$ in., $b = 3.5777$ in.

Each half-elliptic cylinder was machined along its joining edges with a high-speed air router while the cylinder was mounted on the forming mandrel. Two halves were then bonded together with PVC adhesive (Cadco No. 201 solvent cement).

The models were cut to the proper length by mounting them on the center post of the test fixture with the end supports located at the desired length. The center post was then mounted between centers on a lathe and the material extending beyond the end supports was cut off using a high-speed air router. Eighty models were fabricated in this fashion with various geometries which are summarized in Tables 2 and 3.

During tests, the models were held on a fixture with their ends supported by thick aluminum plates which were tapered to a knife edge along their periphery. The models were sealed to the end supports with a thin coat of rubber cement. Hence, we may say that the test models approximately satisfy the end conditions given by Eq. (12) although the fulfillment of the second and third conditions (i.e., $T_x = 0$ and $v = 0$) depends on the amount of friction between the shell and the support.

External pressure was applied by evacuating the air from the interior of the models. The pressure was monitored with a differential pressure transducer whose output operated one channel of an X-Y recorder.

The normal deflections at the midlength of the elliptic cylinder and at the semiminor axis were monitored with displacement transducers whose outputs operated the other channels of the X-Y recorder. Thus, a continuous history of deflection versus external pressure was obtained during a buckling test. Figure 5 shows typical plots of such a history.

The models contained a core made of rigid urethane foam which was smaller than the cylinder. This core prevented the models from completely collapsing when buckling occurred and allowed the shells to buckle elastically so that they could be shortened and retested. It also permitted the buckle pattern to be observed and drawn on the models for a permanent photographic record (Fig. 4). The failure mode for all the models tested appeared to be an oval dimple, situated near the semiminor axis, and had a half-sine wave in the axial direction.

The buckling pressures thus obtained for all the 80 models are recorded in Tables 2 and 3. The physical significance of the rest results will be discussed in the next section.

Discussion of Theoretical and Testing Results

Before this investigation was started, we were tempted to see whether the elliptic shell would buckle at the same pressure as a circular cylinder if the radius of the circular cylinder were equal to the radius of curvature r of the ellipse at its

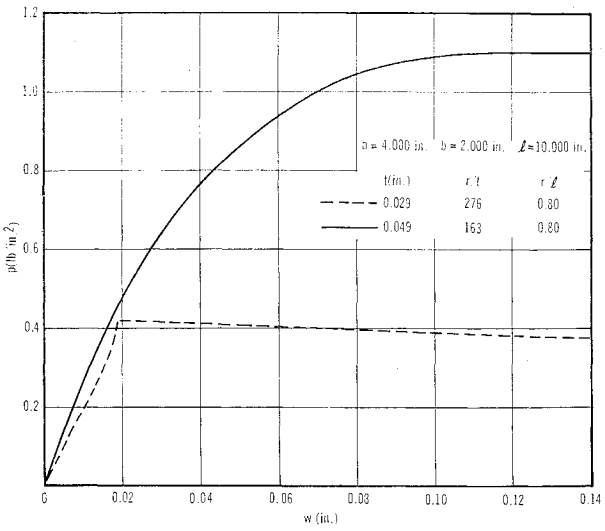

Fig. 5 Deflection vs external pressure ($x = \frac{1}{2}$, $s = 0$).

minor axis.** For purposes of comparison, we made all the test models with r equal to 8 in. Hence, the equivalent circular cylinder also had a radius equal to 8 in.

The solution for the nondimensionalized buckling parameter λ was computed according to the system of Eqs. (14–16). The governing parameters were found as ν, a/b, a/t, and a/l. Since $r = a^2/b$, we preferred to use the following input parameters: $(a/t)(a/b) = r/t$; $(a/l)(a/b) = r/l$ for any fixed values of a/b and ν.

The numerical results based on $\nu = 0.37$ (i.e., Poisson's ratio for the PVC material) and the ratios $a/b = 2.0$ and 1.5 are plotted in Figs. 6 and 7, respectively. These analytical results are also listed with the test data in Tables 2 and 3. It was found that the curves in Fig. 6 with $a/b = 2.0$ are only slightly higher than those in Fig. 7 with $a/b = 1.5$; however, this does not mean that λ will not change significantly as a/b becomes smaller. For $a/b = 1.0$, the cylinder becomes circular and its r/t and r/l ratios become the radius-thickness ratio and the radius-length ratio, respectively. In this particular case, the computer result based on the present theory agrees numerically with the classical von Mises solution for cylindrical shells.[5] The von Mises solution is also plotted with the same parameters and is shown in Figs. 6 and 7 by dotted curves. It is seen that the equivalent circular cylinder solution yields substantially lower buckling values than the present theory. This was expected because the elliptic cylinder is stiffer than the circular cylinder.

Table 4 Ratio of λ_6/λ_{10}

				$a/b = 2.0$				
t, in.	0.018	0.019	0.028	0.029	0.049	0.051	0.090	0.091
λ_6/λ_{10}	1.00	1.02	1.16	0.96	1.09	1.16	1.04	1.05
				$a/b = 1.5$				
t, in.	0.018	0.019	0.029	0.029	0.047	0.049	0.090	0.088
λ_6/λ_{10}	0.98	0.96	0.90	0.90	0.97	0.94	1.00	1.00

It was found theoretically that except for very short shells ($r/l \geq 4.0$ for $a/b = 2.0$ and $a/b = 1.5$), the buckling parameter λ (not pressure p) is relatively insensitive to the r/l ratio. The theoretical values in Tables 2 and 3 illustrate this insensitivity. For this reason, the numerical data of the group for r/l from 0.8 to 2.0 are represented, both in Figs. 6 and 7, by a single curve.

The test data given in Tables 2 and 3 also indicate that the buckling parameter λ is not sensitive to the r/l ratio. To look into this matter further, we defined the λ for the 6-in. cylinder as λ_6 and the λ for the 10-in. cylinder as λ_{10}, and we computed the ratio λ_6/λ_{10} from the test data provided by Tables 2 and 3. These ratios for shells of different thicknesses are given in Table 4.

It is seen that, in most cases, the difference in ratios is no more than 5% with some values of λ_{10} actually even larger than λ_6. Allowing for some experimental error and geometric deviation of models, we may say that both theoretical and test results indicate that for shells of moderate and long length, ($r/l < 2.0$) the buckling parameter λ is indeed relatively insensitive to the r/l ratio.

Figures 6 and 7 also suggest that the test data and theory agree fairly well for the range $r/l = 0.8 \sim 2.0$ and $r/t \geq 200$ in Fig. 6, and for the same r/l but with $r/t \geq 150$ in Fig. 7. Tables 2 and 3 show that within these ranges, the difference between theory and test data is no more than 13%. If we recall the spread of test data reported by various authors for the case of circular cylindrical shells, this difference is not excessive. Comparison of the test data and Figs. 6 and 7 shows that the equivalent circular theory provides a lower bound in this range, while outside it and toward a lower r/t ratio, test data again fall below that theory.††

In Fig. 6 the agreement between theory and test data deteriorates for all values of r/l when $r/t < 200$ and for $r/l \geq 4.0$

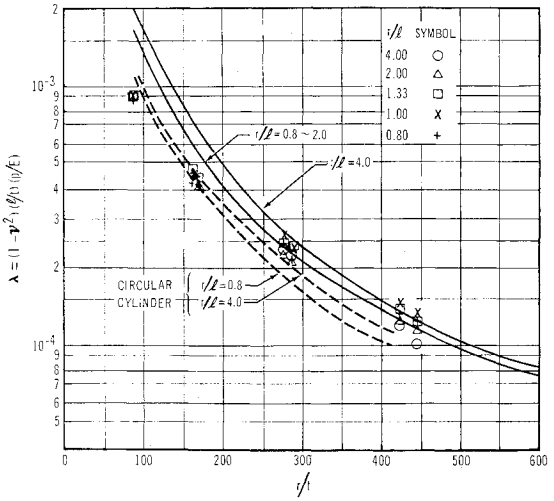

Fig. 6 Buckling parameter λ vs r/t ($a/b = 2.0$, $\nu = 0.37$).

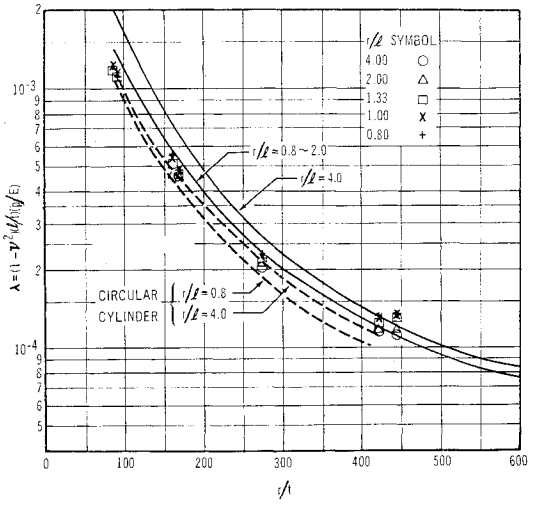

Fig. 7 Buckling parameter λ vs r/t ($a/b = 1.5$, $\nu = 0.37$).

** An interesting remark about the axial compression case is made on p. 460, Ref. 5.

†† We note that equivalent cylinder theory yields good lower bound for axial compression buckling.[7]

Table 5 Eigenvectors for w displacement

n	C_n	n	C_n	n	C_n
2	0.0005	7	0.0016	12	0.905
3	0.00001	8	0.478	13	0.002
4	0.008	9	0.0043	14	0.394
5	0.0002	10	1.00	15	0.0003
6	0.10	11	0.0047	16	0.08

for all values of r/t. The same situation exists in Fig. 7 also for all values of r/l when $r/t < 150$ and for $r/l \geq 4.0$ for all values of r/t. It is apparent that in these ranges either the shell is shorter‡‡ or thicker, or both shorter and thicker. In other words, the shell gets stiffer in these cases. The experimental deflection-pressure curves in this region consistently show that these stiff shells buckled with deflections as large as two and one-half times their thickness (solid curve in Fig. 5) while other models outside this region failed at a much smaller deformation (dotted curve in Fig. 5).

It is understood that the present small deflection theory does not apply to the group of shells which buckled at large deformation as mentioned earlier. Donnell[8] showed that a short, thin, circular cylinder under external pressure buckles at 70% of von Mises solution. He further showed by nonlinear solution that the use of an unevenness factor of $U = 0.0001$ causes the theoretical value to match the test data. Although this paper deals with a different problem, a similar situation may exist. For this reason, it is recommended that the theoretical results be used with discrimination for all the cases with $r/l > 2$ and the case with $r/t < 200$ for $a/b = 2.0$ and $r/t < 150$ for $a/b = 1.5$.

All the numerical results presented so far are based on Poisson's ratio $\nu = 0.37$. Additional calculations show that the values of λ with $\nu = 0.3$ are almost consistently larger by 1% than their counterpart with $\nu = 0.37$. Hence, the λ for any other ν inbetween 0.3 and 0.37 may be obtained by interpolation.

As students and practitioners of buckling analysis, we are also interested in the comparison of the theoretical and test buckling modes. For this purpose, we give the eigenvectors of such modes for a typical case with $r/l = 2.0$, $r/t = 600$, $a/b = 1.5$. Its vector components for w displacement as contributed by the nth term in Eq. (9) are listed in Table 5.

It shows that the odd n terms make an insignificant contribution to the buckling deformation; that is, the buckling mode is essentially symmetrical both about the major and minor axis. In this particular case, the dominant terms are those with $n = 8$, 10, 12, and 14.

‡‡ For shorter shells, say $r/l \geq 4.0$ or even $r/l \geq 2.0$, we feel that the local bending deformation before buckling may have a significant effect on the buckling load. This is evidenced by the fact that test data in this range were situated further below the theory than the test data of longer shells. This is certainly a subject of interest for further study.

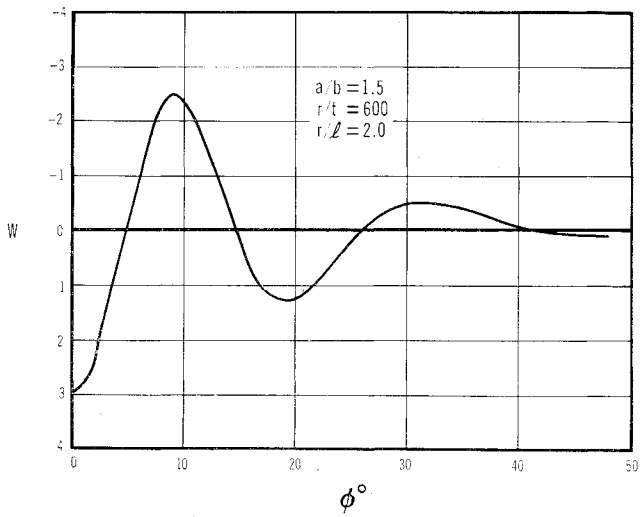

Fig. 8 Buckling mode w vs ϕ.

The resultant buckling mode for w displacement in this particular case is plotted against the normal angle ϕ (Fig. 3) and given in Fig. 8. This mode is similar to the axial compression case.[9] It is seen that theoretically the shell buckles with three troughs on each surface near the minor axis with the dominant trough at the center. The wave dies out after $\phi > 40$ degrees. However, in most experiments, only one trough near the minor axis was noticeable and the buckle pattern only appeared on one side.

References

[1] Slepov, B. I., "Vibrations and Stability of Anisotropic and Sandwich Cylindrical Shells of Arbitrary Cross Section," TT4-341, Oct. 1962, NACA, pp. 826–834.

[2] Goldenveizer, A. L., *Theory of Elastic Thin Shells*, Pergamon Press, New York, 1961, p. 102.

[3] Galerkin, B. G., "Series Solutions of Some Problems of Elastic Equilibrium of Rods and Plates," *Vestnik Inzhenerovi Tekhnikov*, Vol. 1, Vserosslyskaia Assotsiatsiia Inzhenerov, Moscow, 1915, pp. 879–908.

[4] Novozhilov, V. V., *The Theory of Thin Shells*, Noordhoff, Groningen, The Netherlands, 1959, pp. 169–172.

[5] Timoshenko, S., *Theory of Elastic Stability*, McGraw-Hill, New York, 1936, p. 450.

[6] Weingarten, V. I., Morgan, E. J., and Seide, P., "Final Report on Development of Design Criteria for Elastic Stability of Thin Shell Structures," Rept. EM 10-26, 1960, Space Technology Labs., Los Angeles, Calif., p. 158.

[7] Kempner, J., "Some Results on Buckling and Postbuckling of Cylindrical Shells," TND-1510, 1962, NASA, pp. 181 and 186.

[8] Donnell, L. H., "Effect of Imperfections on Buckling of Thin Cylinders Under External Pressure," *Journal of Applied Mechanics*, Vol. 23, No. 24, 1956, p. 575.

[9] Kempner, J. and Chen, Y. N., "Buckling and Postbuckling of An Axially Compressed Oval Cylindrical Shell," *Proceedings of Symposium on The Theory of Shells to Honor L. H. Donnell, University of Houston*, McCutchan, Berkeley, Calif., 1967, p. 162.